Possibilities and limitations of point-contact spectroscopy for measurements of spin polarization

Y. Bugoslavsky, Y. Miyoshi, S. K. Clowes, W. R. Branford, M. Lake, I. Brown, A. D. Caplin, and L. F. Cohen
Blackett Laboratory, Imperial College London, London SW7 2BZ, United Kingdom
(Received 6 August 2004; revised manuscript received 2 December 2004; published 31 March 2005)

Major issues that limit the applicability of point-contact Andreev reflection (PCAR) spectroscopy for measurements of transport spin polarization (P) are investigated. We show that the analysis of the PCAR spectra on the basis of the generalized Blonder-Tinkham-Klapwijk model may lead to degenerate solutions; i.e., the straightforward determination of P from the multiparameter fitting is ambiguous. We have developed a refined method of analysis that reduces the ambiguity. This method is applied to several test cases (copper, NiMnSb, Co_2MnSi, Sr_2FeMoO_6), and it is found to work in materials with low and high P.

DOI: 10.1103/PhysRevB.71.104523 PACS number(s): 74.50.+r, 74.70.Ad, 75.50.Cc

I. INTRODUCTION

Reliable determination of the degree of spin polarization of the transport current is one of the key requirements for the development of spin-polarized materials and ultimately, spintronic devices.[1] Measuring the differential conductance as a function of applied voltage in a microscopic junction between a superconductor and the studied material [i.e., point-contact Andreev reflection (PCAR) spectroscopy] was proposed[2,3] as a relatively simple experimental means of assessing the spin polarization. The benefit of this method is that it directly senses the spin polarization of the transport current, rather than the bare density-of-states polarization.[4] The junction size is usually on the scale of microns, so that the method allows for local measurements. PCAR spectroscopy has been used to characterize various materials ($La_{0.7}Sr_{0.3}MnO_3$,[4] $SrRuO_3$,[5] MnAs,[6] CrO_2,[7,8] $Co_2Cr_{0.6}Fe_{0.4}Al$[9]); however, concerns, both fundamental and technical, have been recognized. The experiments are usually interpreted in terms of the Bardeen-Tinkham-Klapwijk (BTK) model,[10] which was generalized by Mazin, Golubov, and Nadgorny to take into account the effects of spin polarization.[11] Principally, the BTK model considers a contact between two metals with equal Fermi velocities, but Zutic and Valls demonstrated[12] that the Fermi velocity mismatch can lead to significant changes in the spectra. First-principle calculations of the electronic transport across a metal-superconductor interface[13] shows that the BTK model indeed yields a very good approximation to the shape of conductance spectra, albeit the effective barrier parameter Z is related to the microscopic properties in a nontrivial way. Commonly, there is a remarkable agreement between the experiment and generalized BTK model; hence these fundamental issues, although important, do not necessarily impair the validity of the technique.

The parameters used in the generalized BTK are the superconducting gap (Δ), the effective dimensionless potential barrier at the interface (Z), the degree of polarization (P), and the generic spectral broadening (ω). Whether P is sensitive to the probe being in the ballistic or diffusive regime is still a point of discussion.[9,14] Technically speaking, the possibility to obtain a well matched fit can be misleading in a more general sense, as the results of fitting to a four-parameter model conductance may be ambiguous. In spite of much work done on the basis of the PCAR method, the issues related to the uniqueness of the BTK fit and the accuracy and reliability of the values extracted from the fit have not been scrutinized. The focus of the current work is to identify major potential pitfalls and to develop an analysis protocol that provides for accurate interpretation of the data. We investigate the modified BTK model,[11] and determine the range of applicability of the model to the analysis of experimental data. We study a number of materials that are anticipated to have different degrees of spin polarization, starting with copper, to check how reliable the model is in the case wherein the value of P is known to be zero. Data from NiMnSb, Co_2MnSi, and Sr_2FeMoO_6 (SFMO) are also studied. To study the convergence and uniqueness of the fit, we generated a large number of theoretical spectra and fitted them using the same protocol as for the experimental data. The results of simulations will be presented along with the experiments. We develop a computational method that deals efficiently with the nearly degenerate regime of the fitting. We also discuss the implication of applying either ballistic or diffusive BTK formulae to the analysis. Finally, we highlight the potential error produced in normalization of the experimental data, and suggest a method to minimize this problem.

II. EXPERIMENTAL AND COMPUTATIONAL DETAILS

The point contacts were made by pressing a sharp niobium tip to the sample surface. The tips were made of 99.9% pure niobium wire, 0.25 mm in diameter. From the rather high value of the upper critical field ($\mu_0 H_{c2} \sim 800$ mT at 4.2 K), and the mechanical hardness, we can conclude that the material of the cold-worked wire has a high density of defects, which may in part explain the reduced values of the superconducting gap we measure (see below). Tips were sharpened by several oblique scalpel cuts. The apex of an as-sharpened tip is typically about a few microns in size. However, due to the pressure necessary to establish a stable low-resistance junction, the tip is squashed against the sample surface so that the junction is about 50 μm in diameter, as estimated from scanning electron microscope images of the tip taken before and after the measurement. Despite

the large contact area, some of the data are only consistent with the ballistic regime of the BTK theory,[11] which requires the junction size to be smaller than the mean free path in the metal. We therefore assume that our contacts contain a number of much smaller actual point junctions, and that the measured spectra are superpositions of the characteristics of individual points. The variation in the properties of these parallel point contacts can well be a contributing factor to the nonthermal line broadening, as will be discussed later.

A technical problem in the experiment arises when the resistance of the investigated sample is comparable to, or greater than, the resistance of the junction.[14] In this case, a part of the sample adjacent to the point contact contributes to both measured bias and conductance. As a result, the bias scale of a spectrum becomes stretched, and the conductivity features are reduced in amplitude. To avoid further ambiguities in the problem, in this work we present data obtained only on low-resistance samples, where the junction resistance was much greater than the sample resistance, so that the rescaling effect can be neglected.

All measurements reported here were made at the temperature of 4.2 K with the sample stage immersed in liquid helium. The vertical movement of the tip was by means of a stepper motor/gearbox assembly at the top of the inset, a shaft that transmits the motion to the cold sample stage, and a differential screw that actuates the tip. The tip is brought into contact with the sample when in liquid helium, and subsequently the tip is driven further towards the sample so that pressure can be built up at the junction due to the stiffness of the niobium wire. By gradually increasing the pressure it is possible to vary the junction resistance. The physical reason for this variation is at least twofold. Firstly, the tip can crush through the natural surface oxide layer and can hence reduce the interface barrier. Secondly, the area of the junction spot increases as the tip is progressively squashed, also contributing to the reduction of the junction resistance. There is no straightforward way of differentiating between the two effects; however, we will show that the analysis of data taken at the same location on the sample, but with varying tip pressure, proves useful.

The common way of analyzing the PCAR spectra is by finding the best fit to a theoretical generalized BTK dependence, and extracting the values of parameters from the fitting procedure. We have found that all the four parameters (Δ, Z, P, ω) can show significant variation between experiments, so that they all need to be treated as variables. The physical reasons for this variability are discussed in the next section.

In theory, the finite-temperature spectra are calculated by convoluting zero-temperature curves with the derivative of the Fermi distribution function, $-\partial f/\partial E$, which is a peaked function with the half-width equal to $k_B T$ (the product of Boltzmann constant and the temperature). However, the experimental broadening is often considerably larger than $k_B T$, suggesting that interface scattering that breaks the electron coherence plays a significant role. The associated functional form to describe the effect of scattering is unknown. To account for the combined effect of all broadening mechanisms, we take the convolution function in the form of a Gaussian. For convenience, we write the Gaussian as $\exp\{-[(E-E')/2\omega]^2\}$. With such notation, when only the thermal effect is present, the Gaussian approximates $-\partial f/\partial E$, so that $\omega = k_B T$.

The fitting procedure we use is based on an optimization algorithm with the target function being the normalized sum of squared deviations between the fitted data and the trial function:

$$\chi^2(\Delta, Z, P, \omega) = \frac{1}{N}\sum_i [g_i - G(V_i; \Delta, Z, P, \omega)]^2,$$

where the analyzed conductance-voltage $[g(V)]$ curve is comprised of N points (V_i, g_i), and the fitting function $G(V_i)$ is computed in either ballistic or diffusive regime of the generalized BTK. It was found practical to use the bias range from −8 to 8 mV. The algorithm allows us to optimize in all four parameters, or in any subset, while the others are kept fixed. We imposed natural physical constraints on the parameters, keeping them always positive.

The relative noise in our experimental data is typically on the level of 0.3%; this statistical scatter results in the minimum value of χ^2 (on the order of 10^{-5}). To justify the position of the minimum, we need to vary the parameters and gauge the response in χ^2. The systematic variation of χ^2 can be resolved at the level of 1/10 of the statistically limited value, and we assume that attempting to resolve features in χ^2 on the scale smaller than 10^{-6} would be in excess of the overall precision of the analysis. The statistical component of χ^2 is not important for finding the position of the minimum. In the simulated data this component is obviously zero. Therefore, in the following, when reporting the variation of χ^2 as a function of the model parameters, we concentrate on the variable part only; i.e., subtract a constant on the order of 10^{-6}. This helps to bring the quality of fit for experimental and simulated data to a similar scale.

We have found that in certain cases the target function lacks a unique minimum, and the full four-parameter fit becomes degenerate. It is then useful to fix the polarization at a certain value (P_{trial}), run the three-parameter optimization (which is always robust), and obtain the corresponding value of the target function at the minimum (χ^2_{min}). Running this procedure with different values of P_{trial} yields a one-dimensional function $\chi^2_{min}(P_{trial})$, or $\chi^2(P)$ for short, which is useful for understanding the convergence properties of the problem.

III. RESULTS AND DISCUSSION

A. Zero polarization: Copper

First we study the properties of the point contacts with a nonpolarized material. The key question here is whether the behavior of the superconducting tip is predictable enough to consider some of the BTK parameters well fixed to their nominal values. If this were the case, reducing the number of variables would increase the robustness of the fitting procedure. We have, however, found that not only Z, but also Δ and ω are strongly contact dependent, in spite of the fact that the same grade of niobium is used throughout and all the experiments are taken in the liquid helium bath.

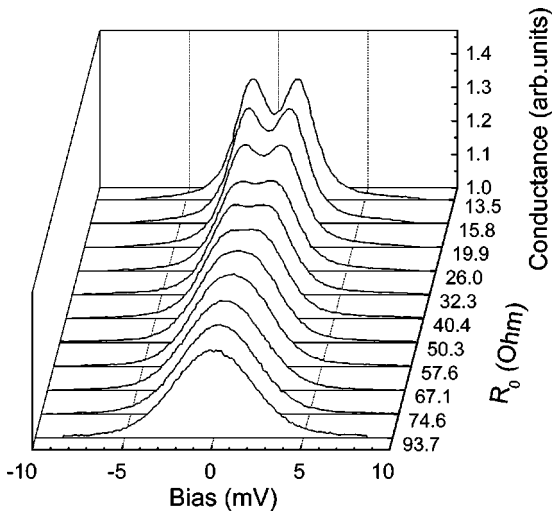

FIG. 1. Point-contact spectra at 4.2 K of a junction between the epitaxial copper film and a niobium tip. Different curves correspond to different junction resistance R_0. The series was started with the lowest-resistance curve, subsequent data were obtained as the pressure on the contact was reduced; similar series were obtained with the reverse direction of tip movement.

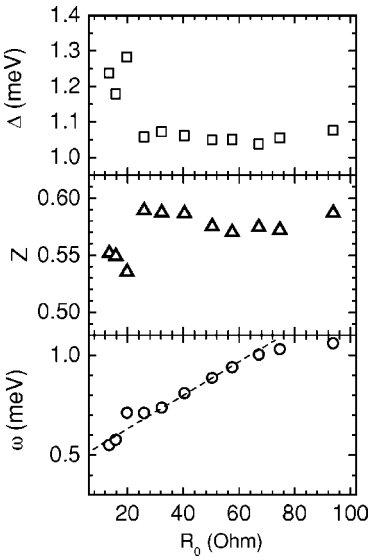

FIG. 2. Parameters of the BTK model for the data of Fig. 1 as functions of the junction resistance R_0.

We obtained a large number of point contacts between niobium tips and an epitaxial copper film deposited on a silicon substrate. There was no special surface treatment prior to the measurements, and the contacts generally have nonzero (although not very large) Z, due to thin oxide layers on copper or niobium. In order to study the variation of contact properties, the conductance spectra were taken sequentially as the pressure on the tip varied while the tip was at the same location on the film. In this way it was possible to obtain a series of spectra, typically spanning the range of background resistance R_0 from 10 to 100 Ω (see Fig. 1).

To demonstrate the variability of junction properties, we present in Fig. 1 a series of spectra, which were taken in a continuous run as the tip pressure was sequentially reduced. For these data, the ballistic regime of the BTK is the only possible choice for modeling. The diffusive simulation, even in the extreme limit of zero Z and zero P, is significantly lower than for the experimental data. The three-parameter fitting is robust with all the curves, and the fitting parameters are shown in Fig. 2. The fact that the value of Δ is noticeably smaller than the gap of bulk niobium ($\Delta_{Nb}=1.5$ meV) suggests that the properties of the tip end are different from the bulk material, probably due to strong plastic deformations and high density of dislocations. Any systematic dependence of the local Δ on contact resistance is difficult to discern in the low-R_0 regime, nor does Z increase monotonically with R_0, most probably reflecting the variation of contact area with pressure. In contrast, the line broadening ω increases consistently with R_0. Even for the low-resistance junction, ω is larger than the purely thermal broadening would be (for the thermal broadening $\omega=K_BT=0.36$ meV at $T=4.2$ K), and the nonthermal contribution increases rapidly with R_0. We note that this dependence is clear evidence that the excess smearing does not originate from local heating at the contact. At a given bias voltage the Joule heating is inversely proportional to R_0, and thus should be more significant for low-resistance contacts, contrary to what is observed. In agreement with this is an order-of-magnitude estimate of a possible local temperature rise at the contact. Assuming that the major heat conduction channel is through the sample (in our case, through the substrate of the copper film), the temperature rise can be estimated as $\Delta T \sim W/(\lambda r)$, where W is the heat power, λ the thermal conductivity and r the radius of the contact. For a film on a sapphire substrate ($\lambda=297$ W m^{-1} K^{-1} at 4 K[15]) and the junction with radius 10 μm and resistance of 10 Ω, the associated temperature rise is on the order of 1 mK at 10 mV bias.

We therefore conclude that the excess smearing is of a nonthermal nature. The correlation it shows with the interface resistance suggests that interface scattering is a likely mechanism that contributes to both the effective transparency and decoherence of the Andreev process. Although further details of this scattering are difficult to obtain from our experiment, the important implication is that low-resistance junctions are required for good spectral resolution.

The conclusion from the results of Fig. 2 is that generally all the parameters of the BTK model need to considered as variables and, to extract the spin polarization, the full four-parameter procedure needs to be used. The issues of uniqueness and convergence of the optimization should therefore be analyzed.

To do so, we ran the full four-parameter optimization with the copper data with a view to determining whether the known zero polarization can be accurately inferred from the analysis. We also compare the results on experimental data with those obtained on simulated spectra.

At zero temperature, the theoretical BTK spectra show a very clear distinction between the effects of increased P and increased Z.[11] This is, however, no longer the case when the spectral broadening becomes significant. Indeed, a broadened theoretical curve generated for a set of parameters can be very closely fitted by another curve, with different values of parameters. An example of a close match between two

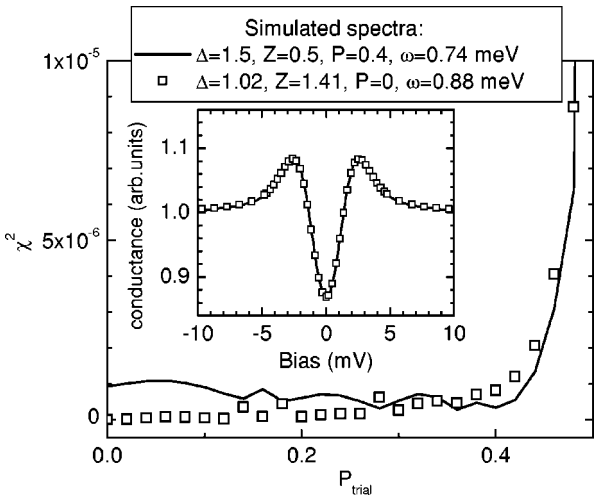

FIG. 3. The inset shows two generated curves that are closely coincident in spite of the polarizations being 0.4 and 0, respectively. For relatively strongly broadened spectra, degenerate fits can be produced by simultaneously varying three fitting parameters: Δ, Z, and ω. Main panel: Results of the χ^2 (P_{trial}) analysis for the two curves. Although there are strict minima that correspond to correct values of P, the total variation in χ^2 is minute below $P_{trial}=0.4$.

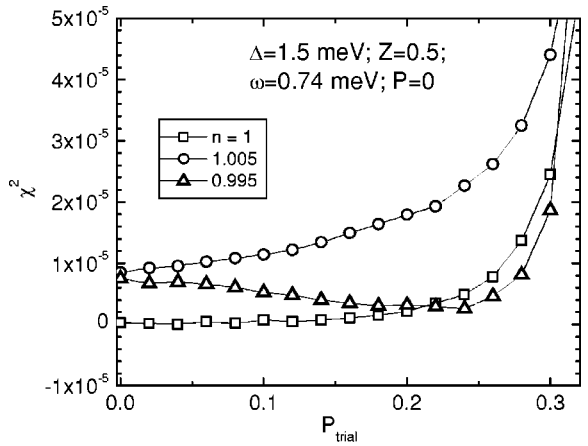

FIG. 4. The effect of spectrum normalization on the convergence of the fitting procedure for a generated spectrum with $P=0$. A 0.5% error in normalization produces a false but robust minimum in χ^2, which would lead to an erroneous inferred polarization of 0.24.

generated curves is shown in the inset of Fig. 3. Strictly speaking, there is a finite difference between the curves, but it is so small ($\chi^2<10^{-7}$) that it would not be possible to discern in the case of the experimental data. The ambiguity is due mainly to the fact that with limited spectral resolution, the model fails to distinguish whether it is high P or high Z that causes the depression of the conductance at small bias.

The degeneracy of the BTK fitting function is a major problem for the applicability of the PCAR method. In the following, we show how the effect of the ambiguity can be reduced.

The main panel of Fig. 3 presents the results of the three-parameter optimization as a function of trial P, computed for the two spectra shown in the inset. The main feature of the $\chi^2(P)$ dependences is a very shallow, almost horizontal part in an extended region of polarization above zero. Although in the mathematical sense the lowest-lying minimum is at $P=0$, it is virtually impossible to resolve within a realistic accuracy of computations and would be totally obscured by even small experimental noise. The horizontal part of the χ^2 represents the compensation effect: the model is able to adjust Z in such a way that it compensates for P and produces virtually equally good fits in a wide range of P_{trial}. The compensation effect extends to higher P as the spectra become more broadened. Beyond a certain value of P_{trial}, there is an abrupt threshold and the quality of fit deteriorates dramatically, indicating that the spectrum becomes incompatible with such high values of P_{trial}. The threshold is a distinct feature that allows one to put an absolute upper limit to a possible value of spin polarization.

Another issue that has an important implication on the data analysis is due to the fact that the experimental data need to be normalized by a high-bias value of conductance: $\sigma_0=1/R_0$. This involves a degree of arbitrary judgment and may be subject to error if there are high-bias conductance features. To check how a small error in the spectrum normalization affects the subsequent analysis, we normalized the simulated curves by 0.995 and 1.005, corresponding to 0.5% experimental uncertainty. The implications on the determination of P are very serious. Figure 4 shows the $\chi^2(P)$ curves for a moderately broadened, zero-polarization theoretical spectrum. The low-P part of the plot is completely transformed for data normalized inappropriately. A spurious slope appears in the graph, which can produce a very well-defined, although artificial, minimum, either at zero P or at a considerably high P, depending on the sign of the error. This minimum becomes the global minimum of the target function, and hence application of the fitting procedure would yield a robust but completely spurious result. In the case when a high-P minimum is present, the actual position of the minimum depends on the interplay of the value of the broadening parameter and the degree of error in σ_0. As Fig. 4 demonstrates, for a reasonable value of ω, only a 0.5% error in normalization may lead to a significant error in interpretation of the data: in case of underestimated σ_0 the four-parameter optimization converges to $P=0.24$ instead of the true value of $P=0$.

We propose a solution to avoid this potentially large error. In Fig. 4 the correctly normalized data yield a zero slope at $P=0$, whereas positive or negative error results in an accordingly positive or negative slope. This fact can be understood on the basis of a simple argument given in the Appendix. Hence, if the correct value of σ_0 was unknown, it could be found by an iterative process aimed at producing a $\chi^2(P)$ curve with zero derivative at $P=0$.

In Fig. 5 we show the experimental lowest-resistance spectrum for the copper sample, normalized according to this procedure. The experimental data lack horizontal background at high bias, due to the presence of shallow conductance minimums. However, with the requirement that the derivative of χ^2 with respect to P_{trial} is zero, our procedure results in the normalization which appears intuitively correct, and the data then yield the expected zero polarization as the result of the complete analysis.

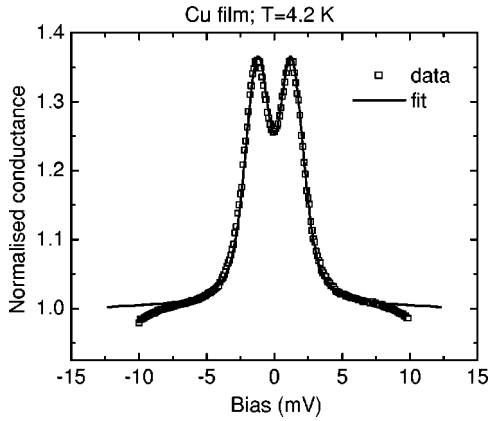

FIG. 5. Experimental normalized spectrum for copper (lowest background resistance curve of Fig. 1; points). The distortions of the spectrum due to the presence of minimums at high bias are efficiently compensated so that the resulting fit (solid line) corresponds to zero polarization.

Due to the fact that the minimum in χ^2 is shallow, and becomes increasingly so as the spectrum becomes more broadened (Fig. 6), the values of fit parameters can be only extracted with a limited accuracy. For the best-resolved spectrum, the upper boundary for P can be put at 0.1, but as the spectrum becomes so broadened that the double-peak structure is not resolved (at $R_0 \sim 40\ \Omega$ in this case), the accuracy deteriorates to such an extent that only the abrupt increase of χ^2 at $P_{trial} \sim 0.4$ can be taken as a solid feature to mark the upper boundary for the polarization of the material. The rapid breakdown of the fitting at these high P_{trial} is associated with the value of Z becoming zero. In other words, when P_{trial} is too high, the compensation effect can no longer work as Z cannot become negative.

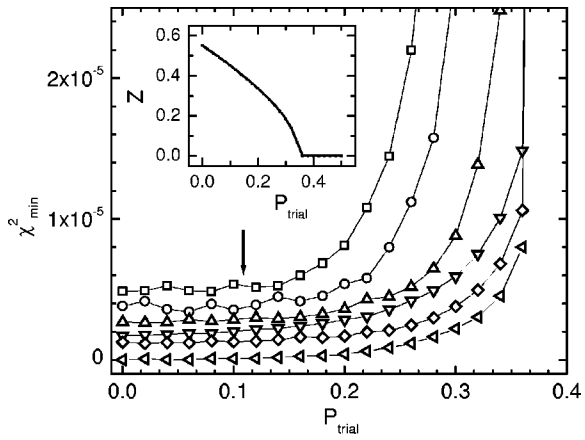

FIG. 6. Results of $\chi^2(P)$ analysis for the differently broadened copper spectra of Fig. 1. The curves are shifted vertically for clarity. The upper limit for intrinsic polarization can be estimated from the onset point on the graph (arrowed). This overestimates the true value by an amount depending on the broadening, but typically by no more than 0.1. The inset shows the values of Z that deliver minimum to the target function at different fixed P_{trial}, for the most broadened spectrum (the bottom curve of the main panel).

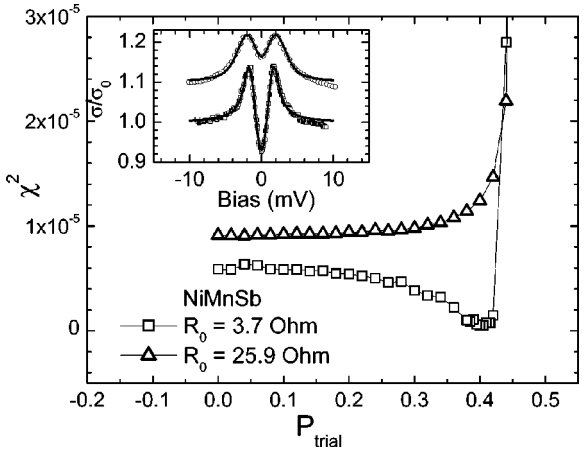

FIG. 7. Inset: Representative spectra for NiMnSb (points) and their best fits (lines). The contact resistances are 3.7 and 25.9 Ω, for the bottom and top curves, respectively. The top curves are shifted vertically for clarity. The broadening parameter for the bottom spectrum is 0.4 meV (equivalent to 4.6 K) and the polarization is 0.4. The top spectrum has excessive broadening of 0.95 meV, and only an upper bound for P can be strictly evaluated, $P_{max}=0.18$.

B. Intermediate polarization: NiMnSb and Co_2MnSi

Nickel manganese antimonide is a half-metal according to band structure calculations,[16] and it has an important technological advantage of being well lattice matched with narrow-gap semiconductor InAs. Therefore, NiMnSb may be potentially suitable for spin injection in hybrid spintronic devices.[17] We apply the procedure discussed above to a series of spectra that were taken at the same location on the sample but at different tip pressures. Two representative spectra for a bulk ingot NiMnSb are shown in inset to Fig 7. As with copper, there are additional spectral features at high bias, and the spectra are not perfectly symmetric; hence correct normalization is an issue.

The results of the analysis of these spectra are shown in the main panel of Fig. 7 (we limit the analysis to the ballistic regime only, for the sake of conciseness). As with the copper data, a small error in normalizing the conductance introduced a significant slope in the $\chi^2(P)$ curve, which is sufficient to distort the minimum. Requiring that the slope of $\chi^2(P)$ is zero at zero P provides an efficient algorithm for finding the normalization constant for each spectrum with adequate precision.

The results for the broad spectrum show that the onset of χ^2 increase is at about $P=0.15$. The absence of a well-defined minimum in χ^2 indicates that these data qualitatively fall in the same regime of effective P-Z compensation as broadened copper data, and hence only an upper bound for P can be evaluated. However, the well-resolved spectrum does produce a minimum at $P=0.4$, albeit asymmetric and with a shallow slope at the left-hand side.

The parameters extracted from the fitting for a number of curves are presented in Fig. 8. Where the fit is robust, the values of the parameters are shown as points; otherwise, only the upper bound for P (and, correspondingly, upper bound for Δ and lower bounds for Z and ω) can be determined.

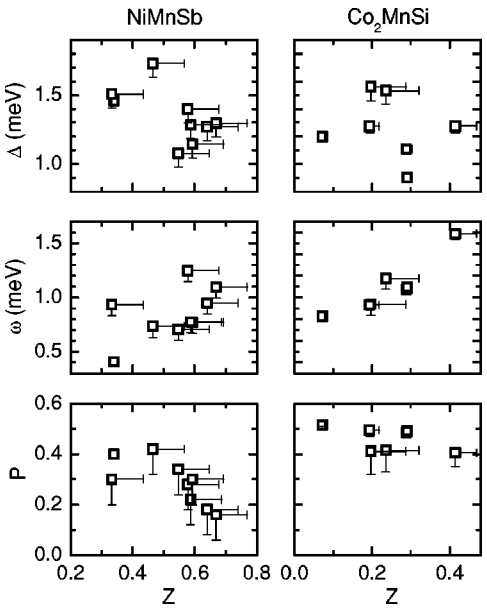

FIG. 8. Left: The BTK parameters of NiMnSb/Nb point contacts. In these plots points with the smallest ω correspond to the bottom curve of inset, Fig. 7. Right: parameters as obtained for point-contact spectra of the Co_2MnSi film. The error bars to one side of a point indicate that the point represents an upper/lower bound for the respective parameter. Where a solution to the fitting problem is unique, the error bars are not shown.

Although semiquantitative for a large proportion of the data, this analysis provides a useful insight into the properties of the material and the interface. The transport spin polarization at the surface of NiMnSb is clearly much smaller than the theoretically predicted 100%. This is likely to be attributable to strong detrimental effect of small off-stoichiometry, as discussed in our earlier paper.[17] Interestingly, there is a correlation between the BTK barrier Z and line broadening ω, indicative of the fact that higher barriers cause stronger interface scattering. Increasing broadening also correlates with reduced polarization, therefore, spin-flip scattering must play a role.

Another potentially highly spin-polarized material is a full Heusler alloy cobalt manganese silicide, Co_2MnSi. We have obtained PCAR spectra on several epitaxial thin films grown on sapphire substrates; the details of film preparation were given elsewhere.[18] Qualitatively, the results are similar to NiMnSb in that the polarization is noticeably lower than 100%, and the P-Z compensation makes the determination of P difficult. Even so, application of the described procedure (using the ballistic regime) results in a $\chi^2(P)$ curve with a shallow minimum corresponding to P in the range between 0.4 and 0.5. The minimum disappears for broadened data, so that in the high-Z, high-ω regime, only upper/lower limits for the parameters can be estimated. Comparing these results for Co_2MnSi and NiMnSb with those shown in Fig. 8, we conclude that the correlation between Z and ω, as well as the decay of polarization in high-barrier contacts, are generic properties of the interfaces with point contacts.

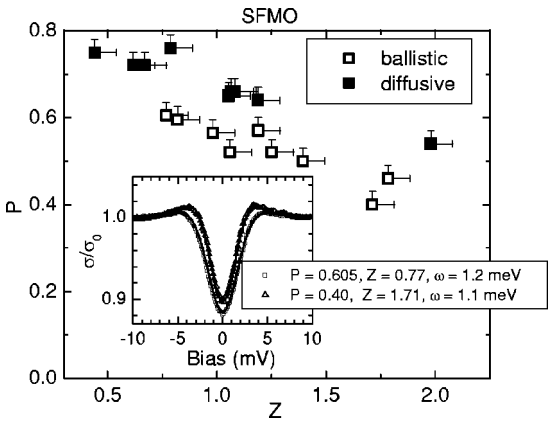

FIG. 9. Main panel: Polarization vs the barrier strength, as inferred from fitting of the SFMO spectra. Open and filled symbols correspond to ballistic and diffusive regimes on the generalized BTK theory, respectively. Inset: Experimental spectra for the SFMO film and their respective best fits. The distinct effect of higher polarization is the reduction of the amplitude of the conductance peaks.

C. High polarization: SFMO

A double-perovskite complex oxide Sr_2FeMoO_6 (SFMO) is being studied intensively for its potential device applications. High-quality, highly aligned films of SFMO were grown at Imperial College by a chemical-vapor process.[19] The point-contact spectra of an SFMO film (inset, Fig. 9) are quantitatively different from the other materials in this paper in that the minimum at zero bias is deeper, and the maximums are nearly absent. However, the broadening is considerable, so that it is not straightforward to decide whether the shape of the spectrum is due to high P or due to an enhanced barrier Z.

The χ^2 versus P analysis yields very different results as well. The shape of the curve now depends on whether we trace it with increasing or decreasing P_{trial} (Fig. 10). This is a clear indication that the target function has multiple local minimums and the optimization procedure converges to a particular minimum depending on the starting values of the parameters. When the starting values for the next trial P are taken as the result of the optimization at previous trial P, we can force the system to stay within a particular valley on the χ^2 (Z, Δ, P, ω) surface. In this way we can obtain trajectories that trace the valleys. The trajectory can be visualized by plotting a projection on the P-Z plane. In the top panel of Fig. 10 we plot two trajectories corresponding to the two branches of $\chi^2(P)$ dependence shown in the bottom panel. As P increases, the system experiences a bifurcation, and the trajectory splits into two branches. The lower branch (which is a visual continuation of the line at lower P) corresponds to the symmetric parabolic branch of χ^2. When on the upper branch (increasing Z with increasing P), the system falls into a compensation regime, similar to the low-polarization case of the previous sections. When the polarization is high, the further increase of P can be compensated by increasing Z.

Interestingly, the bifurcation point lies close to the position of the minimum on the "regular" branch. This means

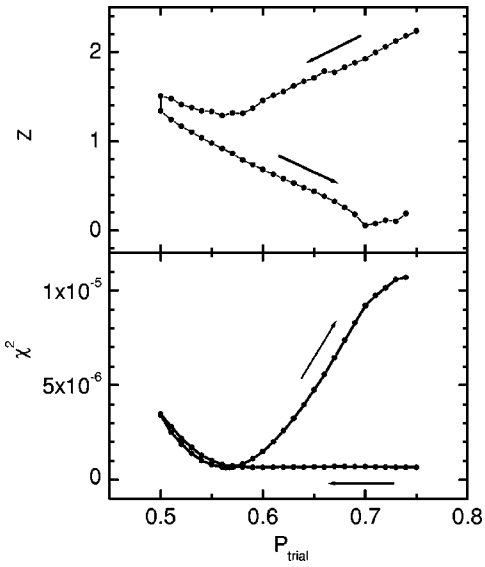

FIG. 10. Bifurcating trajectory of the fitting process for a relatively high-P, high-Z spectrum of SFMO. Depending on whether the trial P is progressively decreased or increased, the system follows different paths which correspond to different local minimums of the χ^2 function. The top panel shows the trajectories in the P-Z plane; the bottom one: the corresponding values of χ^2. The bifurcation point is closely coincident with the minimum of the parabolic branch.

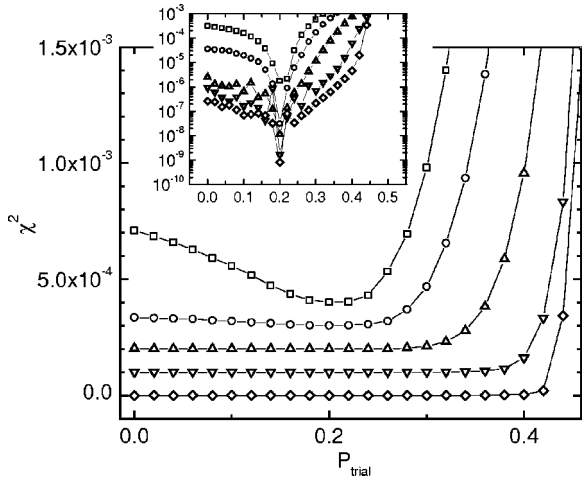

FIG. 11. Results of the three-parameter fit of a theoretical curve with $P=0.2$, $Z=0.5$, in the ballistic regime. The curves correspond to different broadening (top to bottom: $\omega=0.213$ meV (=2.5 K), 0.362 meV (=4.2 K), 0.53, 0.75, and 0.96 meV) and are offset vertically for clarity. The inset presents the same data on a logarithmic scale. Although mathematically all curves have a minimum corresponding to correct value of P, increasing broadening causes the minimum to become progressively more shallow, so that it virtually degenerates into a wide plateau.

that when the trial P is less than the real value of polarization, the $\chi^2(P)$ is a single-valued function. Therefore either the minimum of the parabola or the onset point of the asymmetric "irregular" branch can be taken as a good estimate of P.

For the SFMO data it is possible to apply both ballistic and diffusive limits of the generalized BTK theory. There is little difference between the two regimes in terms of computational properties and the topology of the χ^2 surface. The diffusive regime, however, yields systematically higher values of the extracted spin polarization.

The inferred spin polarization is shown in Fig. 9 as a function of the barrier Z. The highest value obtained within the ballistic regime is 0.6; it increases to 0.75 if the diffusive-limit formulae are used. This observation is in line with recent results of Woods *et al.*,[14] who have shown that the inferred values of P are relatively insensitive to the choice of the ballistic or diffusive regime. We also note that for both regimes, there is an increase in P with decreasing Z, consistent with other measurements.

IV. SUMMARY OF THE SIMULATION RESULTS

In this section we present purely computational results and extend the simulated data to the range of parameters inaccessible in our experiments. Primarily the goal is to determine the effect of line broadening on the robustness of the fitting. The broadening is a combined effect of the temperature and interface scattering, so that the experimental situation corresponding to the discussed simulations is that of an ideally clean interface at 2.5 and 4.2 K, and progressively increasing scattering at $T=4.2$ K. We therefore simulate curves with effective broadening parameters of 0.213 meV (=2.5 K), 0.362 meV (=4.2 K), 0.53, 0.75, and 0.96 meV. The latter three values correspond to the range of ω observed in the experiment.

For each of the above values of ω, we have generated ballistic-limit and diffusive-limit curves for a number of values of P and Z. The behavior of the model was found to be different depending on whether low-P or high-P spectra were fitted.

First we present results for the low-P case ($P=0.2$, $Z=0.5$). As before, we attempt to fit the generated spectrum using a three-parameter procedure with a fixed P_{trial}. The resulting χ^2 dependencies are shown in Fig. 11. For the effective temperature of 2.5 K, there is a very well-defined (although asymmetric) minimum which guarantees convergence. At $T=4.2$ K the minimum becomes significantly more shallow, but it still indicates the presence of a unique well-defined solution. As the broadening increases further, the minimum transforms into a virtually straight horizontal line. Although, strictly speaking, the correct value of P still delivers a minimum to the target function (which can be seen in the inset, Fig 11), the variation of χ^2 on the level of 10^{-7} would be unobservable in the experimental data.

The rapid increase of χ^2 at $P_{trial}>P_0$ marks the breakdown and can be used as an absolute upper bound for P. This estimate depends on Z, though.

When fitting strongly broadened spectra, a serious computational difficulty arises. The relief of the target function becomes complex, with a large number of shallow local minima. The global minimum is well defined and can be found at $\omega<1$ meV, where the additional minimums are relatively more shallow than the global one.

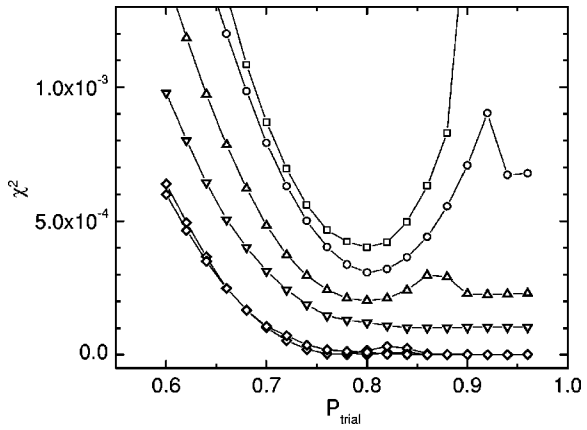

FIG. 12. Similar results for model curves with $P=0.8$ and varying broadening (same as in Fig. 11). The minimums in χ^2 become ill-defined for strongly broadened spectra.

For high P, the system shows some features that we illustrate with the example of $P=0.8$. The $\chi^2(P)$ curves for different broadening parameters are shown in Fig. 12. For $\omega<0.5$ meV there is a good global minimum, although there is a different branch for high P_{trial}. The bottom two curves in Fig. 12 lack a minimum, and indeed the convergence becomes problematic at this high broadening. The lowest curve represents several traces, as obtained by starting the fitting procedure from different values of the parameters. To understand the origin of these noncoincident traces, we plot the variation of Z, which corresponds to the minimum in χ^2 as a function of P_{trial} (Fig. 13). These plots can be seen as trajectories of the system, which run along the valley of local minimums of the function χ^2. Panels (a) and (b) correspond to small broadening, and there is a well-defined single valley that runs through the global minimum at $P=0.8$, $Z=0.5$. However, at high trial P (>0.9) another line of minimums appears and the system bifurcates discontinuously between the two valleys. In panel (c) the bifurcation becomes a rather

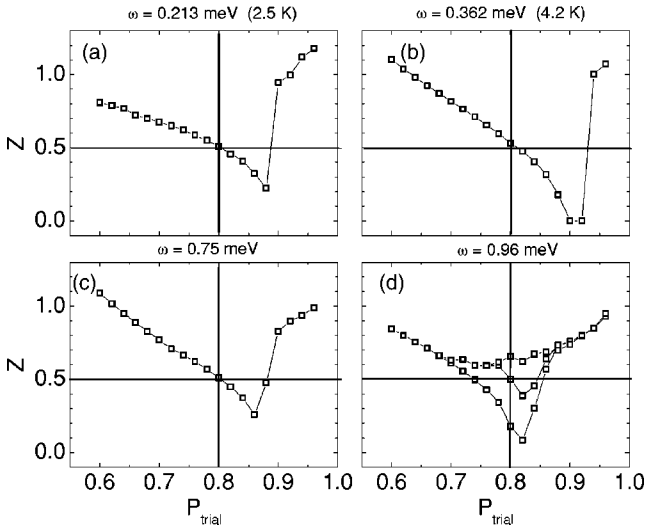

FIG. 13. Demonstration of development of multiple minimums of the target function. The plots represent trajectories that the system follows at the fitting process, projected on P-Z plane.

smooth continuous transition; still, the trajectory remains unique. At high broadening there is a qualitative change. As panel (d) shows, the global minimum becomes surrounded by a triangular system of trajectories that correspond to paths along valleys of local minimums. Which particular path the system takes in this situation depends on the computational details of the algorithm implementation. The presence of many low-lying minimums strongly complicates the analysis and puts the robustness of the results in question. In the case of large broadening, the best that can be expected of the fitting procedure is a semiquantitative estimate of P on the basis of the steep left-hand branch of the $\chi^2(P)$ curve. In this way a lower bound for P can be set.

V. CONCLUSIONS

We have analyzed the issues of applicability of the generalized BTK model to infer the transport spin polarization P from the PCAR spectroscopy data obtained with niobium tips at 4.2 K. It was found that the value of the superconducting gap Δ at the tip apex, as well as the effective interface barrier Z and the spectral broadening ω, all show considerable variability, and therefore all these parameters need to be treated as variables in the optimization problem. Yet another complication is caused by the potentially large error due to the uncertainty of the normalization of the experimental data. The importance of this point stretches far beyond the technical aspect, as incorrect normalization can totally transform the landscape of the χ^2 function, resulting in spurious minimums at high polarization for genuinely zero-polarized data.

The multiparameter fitting problem can be mathematically ill defined; i.e., the χ^2 function may have multiple minimums. We have developed an analysis procedure that allows us to solve the normalization issue separately, and to analyze the convergence in Δ, Z, P, and ω efficiently. The major factor that has a detrimental effect on the convergence is spectral broadening, which is caused by two mechanisms: temperature and interface scattering. At a temperature of 4.2 K, the thermal broadening is small enough for the χ^2 to have a unique single minimum, but the additional broadening due to interface scattering causes the BTK analysis to fail. When this occurs, only a lower or an upper bound for P can be evaluated rather than a precise value.

In the case of low-polarization materials, the effect of the broadening is most crucial, so that only a robust upper bound for P can be inferred from our data. This is sufficient for quick characterization of potentially spin-polarized materials, but experiments at lower temperatures and on higher-quality interfaces are necessary to study subtle effects; e.g., spin diffusion through thin copper films.[20]

Generally, the model is more robust for highly polarized materials. SFMO with the spin polarization of 0.6–0.75 (the two values inferred from using ballistic and diffusive regimes of BTK, respectively) falls into this class. Although the topological features of the χ^2 function may cause problems for strongly broadened spectra, the overall performance of the model is more satisfactory than in the low-P case.

In conclusion, with the recognition of the limitations and by application of the refined analysis protocol, the BTK

model provides a description and a useful tool to infer or to evaluate the spin polarization from point-contact spectra. This further justifies the use of the relatively simple PCAR technique at liquid helium temperature for characterization of ferromagnetic materials. The quality with which the model reproduces the experimental data for a wide range of materials is remarkable. To increase the resolution of the PCAR spectroscopy, better control over the interface is as necessary as working at temperatures below 4.2 K. At this stage it is clear that much better-resolved data are required to discern deviations from the BTK model, for example, due to the effects of Fermi velocity mismatch.

ACKNOWLEDGMENTS

We are grateful to C. Grigorescu, C. Marrow, Z. H. Barber, L. Singh, M. Blamire, J. Rager, and J. L. MacManus-Driscoll for providing us with the samples for this study. This work has been supported by the UK Engineering and Physical Sciences Research Council, National Physical Laboratory and the EU contract FENIKS G5RD-CT-2001-00535.

APPENDIX: NORMALIZATION OF EXPERIMENTAL SPECTRA

As a criterion of the correct normalization, we use the observation that the derivative of $X(P) \equiv \chi^2(P)$ curve at zero P is equal to zero. This property of the fitting procedure can be proved as follows.

Let $G_1(V)$ be the spectrum of a contact with particular values of Z and $P>0$, and $G_2(V)$ the fitting function. Assume that the exact normalization is unknown, so that a function $G_1(1+\alpha)$ is being fitted, where $|\alpha| \ll 1$. We consider the three-parameter fitting with fixed P_{trial} so that the best fit function $G_2{}^0$ delivers minimum to the target function:

$$X(P_{trial}) = \min_{Z,\Delta,\sigma} \int [G_1(V)(1+\alpha) - G_2(V)]^2 dV = \int [G_1(V)(1+\alpha) - G_2^0(P_{trial};V)]^2 dV. \quad \text{(A1)}$$

Due to the degeneracy of the spectra produced by the BTK model at small P, $G_2(P_{trial}=0)$ yields a perfect fit (to within the numerical accuracy) to G_1. However, with $\alpha \neq 0$, the term αG_1 is very dissimilar in shape to the trial function, as the former has very low amplitude at high bias compared to the latter (the ratio is $\alpha:1$).

The slope of the function X is easily obtained by differentiating (A1):

$$\frac{\partial X(P)}{\partial P} = -\int 2[G_1(V)(1+\alpha) - G_2^0(P;V)] \frac{\partial G_2^0}{\partial P} dV. \quad \text{(A2)}$$

At zero temperature and within the gap voltage, the polarized spectrum $G(Z,P)$ is obtained from the classical zero-P BTK function as $G(Z,P)=G_{BTK}(Z)(1-P)$. We extend this relation to approximate the derivative under the integral in (2) as

$$\frac{\partial G_2^0}{\partial P} = -G_{BTK}. \quad \text{(A3)}$$

Due to the close match between G_1 and G_2^0, only one non-negligible term remains in (2):

$$\frac{\partial X(P)}{\partial P} = 2\alpha \int [G_1(V) \cdot G_{BTK}] dV. \quad \text{(A4)}$$

The product of two spectra is always positive; hence the sign and the magnitude of the derivative of X is determined by α. The derivative becomes zero in case of precise normalization; i.e., when $\alpha=0$.

[1] S. A. Wolf, D. D. Awschalom, R. A. Buhrman, J. M. Daughton, S. von Molnar, M. L. Roukes, A. Y. Chtchelkanova, and D. M. Treger, Science **294**, 1488 (2001).
[2] S. K. Upadhyay, A. Palanisami, R. N. Louie, and R. A. Buhrman, Phys. Rev. Lett. **81**, 3247 (1998).
[3] R. J. Soulen, J. M. Byers, M. S. Osofsky, B. Nadgorny, T. Ambrose, S. F. Cheng, P. R. Broussard, C. T. Tanaka, J. Nowak, J. S. Moodera, A. Barry, and J. M. D. Coey, Science **282**, 85 (1998).
[4] B. Nadgorny, I. I. Mazin, M. Osofsky, R. J. Soulen, P. Broussard, R. M. Stroud, D. J. Singh, V. G. Harris, and A. Arsenov, Ya. Mukovskii, Phys. Rev. B **63**, 184433 (2001).
[5] B. Nadgorny, M. S. Osofsky, D. J. Singh, G. T. Woods, R. J. Soulen, M. K. Lee, S. D. Bu, and C. B. Eom, Appl. Phys. Lett. **82**, 427 (2003).
[6] R. P. Panguluri, G. Tsoi, B. Nadgorny, S. H. Chun, N. Samarth, and I. I. Mazin, Phys. Rev. B **68**, 201307 (2003).
[7] Y. Ji, G. J. Strijkers, F. Y. Yang, C. L. Chien, J. M. Byers, A. Anguelouch, G. Xiao, and A. Gupta, Phys. Rev. Lett. **86**, 5585 (2001).
[8] A. Anguelouch, A. Gupta, Gang Xiao, D. W. Abraham, Y. Ji, S. Ingvarsson, and C. L. Chien, Phys. Rev. B **64**, 180408 (2001).
[9] N. Auth, G. Jakob, T. Block, and C. Felser, Phys. Rev. B **68**, 024403 (2003).
[10] G. E. Blonder, M. Tinkham, and T. M. Klapwijk, Phys. Rev. B **25**, 4515 (1982).
[11] I. I. Mazin, A. A. Golubov, and B. Nadgorny, J. Appl. Phys. **89**, 7576 (2001).
[12] I. Zutic and O. T. Valls, Phys. Rev. B **61**, 1555 (2000).
[13] K. Xia, P. J. Kelly, G. E. W. Bauer, and I. Turek, Phys. Rev. Lett. **89**, 166603 (2002).
[14] G. T. Woods, R. J. Soulen, I. I. Mazin, B. Nadgorny, M. Osofsky, J. Sanders, H. Srikanth, W. F. Egelhoff, and R. Datla, Phys. Rev. B **70**, 054416 (2004).
[15] http://www.efunda.com/materials/elements/
[16] R. A. de Groot, F. M. Mueller, P. G. van Engen, and K. H. J. Buschow, Phys. Rev. Lett. **50**, 2024 (1983).
[17] S. K. Clowes, Y. Miyoshi, Y. Bugoslavsky, W. R. Branford, C.

Grigorescu, S. A. Manea, O. Monnereau, and L. F. Cohen, Phys. Rev. B **69**, 214425 (2004).
[18] L. J. Singh, Z. H. Barber, Y. Miyoshi, Y. Bugoslavsky, W. R. Branford, and L. F. Cohen, Appl. Phys. Lett. **84**, 2367 (2004).
[19] J. Rager, A. V. Berenov, L. F. Cohen, W. R. Branford, Y. V. Bugoslavsky, Y. Miyoshi, M. Ardakani, and J. L. MacManus-Driscoll, Appl. Phys. Lett. **81**, 5003 (2002).
[20] S. K. Clowes, Y. Miyoshi, O. Johannson, B. J. Hickey, C. H. Marrows, M. Blamire, W. R. Branford, Y. V. Bugoslavsky, and L. F. Cohen, J. Magn. Magn. Mater. **272–276**, E1471 (2004).